

## CORRELATING INFALL WITH DEUTERIUM FRACTIONATION IN DENSE CORES

SCOTT SCHNEE<sup>1</sup>, NATHAN BRUNETTI<sup>1</sup>, JAMES DI FRANCESCO<sup>2,3</sup>, PAOLA CASELLI<sup>4</sup>, RACHEL FRIESEN<sup>1,5</sup>, DOUG JOHNSTONE<sup>2,3,6</sup>, ANDY PON<sup>2,3,4</sup>

*Draft version July 24, 2018*

### ABSTRACT

We present a survey of HCO<sup>+</sup> (3-2) observations pointed towards dense cores with previous measurements of  $N(\text{N}_2\text{D}^+)/N(\text{N}_2\text{H}^+)$ . Of the 26 cores in this survey, five show the spectroscopic signature of outward motion, nine exhibit neither inward nor outward motion, eleven appear to be infalling, and one is not detected. We compare the degree of deuterium fractionation with infall velocities calculated from the HCO<sup>+</sup> spectra and find that those cores with  $[\text{D}]/[\text{H}] > 0.1$  are more likely to have the signature of inward motions than cores with smaller  $[\text{D}]/[\text{H}]$  ratios. Infall motions are also much more common in cores with masses exceeding their thermal Jeans masses. The fastest infall velocity measured belongs to one of the two protostellar cores in our survey, L1521F, and the observed motions are typically on the order of the sound speed.

*Subject headings:* stars: formation, Stars: protostars

### 1. INTRODUCTION

Starless cores are dense ( $n \sim 10^5 \text{ cm}^{-3}$ ), cold ( $T \sim 10 \text{ K}$ ), and compact ( $r \sim 0.05 \text{ pc}$ ) objects embedded within molecular clouds (Di Francesco et al. 2007). Starless cores are the transition phase between the comparatively diffuse molecular cloud material and a new generation of protostars. The cores are often identified from their (sub)millimeter dust continuum emission and classified as starless from the lack of infrared emission indicative of an embedded protostar (e.g., Nutter & Ward-Thompson 2007; Hatchell et al. 2007; Enoch et al. 2008). Recent (sub)millimeter interferometric observations have shown that low-luminosity protostars have been overlooked by *Spitzer* in roughly 10% of supposedly starless cores (Schnee et al. 2012).

In the cold and dense interiors of starless cores, chemical reactions lead to deuterium enrichment of some molecules that remain in the gas phase, such as N<sub>2</sub>H<sup>+</sup> (see, e.g., Caselli et al. 2008). In a survey of low-mass cores in nearby molecular clouds, Crapsi et al. (2005) measured  $N(\text{N}_2\text{D}^+)/N(\text{N}_2\text{H}^+)$  values ranging from 0.01 to 0.44, much larger than the  $[\text{D}]/[\text{H}]$  elemental abundance of  $\simeq 1.5 \times 10^{-5}$  (Oliveira et al. 2003) found in the ISM. Crapsi et al. (2005) concluded that the  $N(\text{N}_2\text{D}^+)/N(\text{N}_2\text{H}^+)$  ratio is an indicator of core evolution such that a high ratio implies that a core is close to transitioning from being starless to forming a protostar. Friesen et al. (2013) showed that the deuterium

fraction in cores in the Perseus molecular cloud tends to increase with H<sub>2</sub> column density and with increasing core concentration, in agreement with the Crapsi results. Emprechtinger et al. (2009) found that the N<sub>2</sub>D<sup>+</sup>/N<sub>2</sub>H<sup>+</sup> ratio is also an indicator of evolutionary state for Class 0 protostars, with the youngest protostars having the highest deuterium fractionation and clearest signs of ongoing collapse. In the Perseus sample, the most highly deuterated protostellar cores are still associated with significant envelope mass (Friesen et al. 2013). Therefore, in the evolution of a collapsing core, the  $N(\text{N}_2\text{D}^+)/N(\text{N}_2\text{H}^+)$  ratio is expected to peak just as the protostar is formed. In a sample of starless cores, one might expect the N<sub>2</sub>D<sup>+</sup>/N<sub>2</sub>H<sup>+</sup> ratio to be roughly indicative of the likelihood of collapse, with scatter due to differences in core properties such as mass, temperature, non-thermal motions, and magnetic field strength.

Infall and outflow motions in dense cores are revealed by asymmetries in their spectral line profiles. In a simple model of collapse, density, optical depth, and excitation temperature increase towards the center of the core. Inward motions of the side of the core nearer to the observer induce a redshift relative to the average core velocity, and, as a result, one expects to see red-shifted self-absorption of optically thick lines. Myers et al. (1996) and De Vries & Myers (2005) present sets of equations that can be used to derive infall velocity in idealized cases of core velocity and density profiles, and these models match observations with reasonable accuracy. In a real core, the inferred infall velocity depends on the point at which the observed line becomes optically thick and the variation of the infall velocity with radius, complicating the interpretation of the observed spectra. Nevertheless, surveys of infall motions in dense cores have been successfully carried out using various molecular tracers, such as HCO<sup>+</sup> (Gregersen & Evans 2000), HCN (Sohn et al. 2007), CS (Williams & Myers 1999; Lee et al. 1999, 2001), and N<sub>2</sub>H<sup>+</sup> (Williams & Myers 1999; Lee et al. 1999, 2001; Crapsi et al. 2005).

Infall in a starless core will result in a localized density increase due to mass accumulation and a decrease in the central core temperature due to the additional shielding

sschnee@nrao.edu

<sup>1</sup> National Radio Astronomy Observatory, 520 Edgemont Road, Charlottesville, VA 22903, USA

<sup>2</sup> National Research Council Canada, Herzberg Institute of Astrophysics, 5071 West Saanich Road Victoria, BC V9E 2E7, Canada

<sup>3</sup> Department of Physics & Astronomy, University of Victoria, PO Box 3055 STN CSC, Victoria, BC, V8W 3P6, Canada

<sup>4</sup> School of Physics and Astronomy, University of Leeds, Leeds LS2 9JT, UK

<sup>5</sup> Dunlap Institute for Astronomy and Astrophysics, University of Toronto, 50 St. George Street, Toronto M5S 3H4, Ontario, Canada

<sup>6</sup> Joint Astronomy Centre, 660 North A'ohoku Place, University Park, Hilo, HI 96720, USA

from the interstellar radiation field. These conditions promote increased deuteration, so one might expect to see large infall velocities in those cores with the highest degree of deuteration. To test the hypothesis of a correlation between chemical and dynamical evolution, we observed the  $\text{HCO}^+$  (3-2) and  $\text{H}^{13}\text{CO}^+$  (3-2) lines toward every core in the Crapsi et al. (2005) sample for which the  $N(\text{N}_2\text{D}^+)/N(\text{N}_2\text{H}^+)$  ratio was measured. If those cores with the highest  $N(\text{N}_2\text{D}^+)/N(\text{N}_2\text{H}^+)$  ratio are really on the verge of forming a protostar, then we expect them to also show infall signatures. Those cores with smaller observed deuterium enrichment would have slower, or non-existent, infall motions.

Similarly, those cores more massive than their thermal Jeans mass might also be expected to exhibit infall motions. We also compare the observed motions with the Jeans stability of each core to test the hypothesis that those cores with  $M/M_J > 1$  will have inward motions while cores with  $M/M_J < 1$  will appear to be static. More details on this survey are reported below.

## 2. OBSERVATIONS

The 26 dense cores in this survey are those for which the  $N(\text{N}_2\text{D}^+)/N(\text{N}_2\text{H}^+)$  ratios were measured by Crapsi et al. (2005). The Crapsi et al. (2005) sample is meant to be representative of evolved (i.e. dense) starless cores, with their high densities derived from  $\text{N}_2\text{H}^+$  (1-0) or 1.2 mm dust continuum emission. Although thought to be starless by Crapsi et al. (2005), the cores L1521F (Bourke et al. 2006) and L328 (Lee et al. 2009) were later found to be protostellar. The Crapsi et al. (2005) cores are nearby, i.e., within 250 pc, making them comparatively easy to study. We chose to observe  $\text{HCO}^+$  (3-2) to trace inward and outward motions in these dense cores.  $\text{HCO}^+$  (3-2) was shown by Gregersen & Evans (2000) to be a good tracer of line asymmetries in starless cores. The effective critical density of  $\text{HCO}^+$  (3-2),  $6.3 \times 10^4 \text{ cm}^{-3}$  (Evans 1999), is well-matched to the densities of the cores in the Crapsi et al. (2005) sample,  $8 \times 10^4 \text{ cm}^{-3} - 1.4 \times 10^6 \text{ cm}^{-3}$ . The observed spectra are likely to be affected by optical depth and depletion such that  $\text{HCO}^+$  (3-2) may not be tracing exactly the same portion of every core in our sample. Although this source of uncertainty is unavoidable in a survey such as ours, we outline a possible path around this uncertainty in Section 5.

Our observations were centered on the position of the peak  $N(\text{N}_2\text{D}^+)/N(\text{N}_2\text{H}^+)$  given in Crapsi et al. (2005). The  $[\text{N}_2\text{D}^+]/[\text{N}_2\text{H}^+]$  ratio is expected to peak in the region with the highest density and coldest temperature. High densities and low temperatures (and therefore low thermal support) are conditions that are likely to lead to gravitational collapse. The coordinates of our pointed observations and the degree of deuteration are given in Tables 1 and 2. The noise values of the spectra are given in Table 1. The observed  $\text{HCO}^+$  (3-2) spectra are shown in Figures 1a - 1d.

The data were obtained at the James Clerk Maxwell Telescope<sup>7</sup> (JCMT) using the 1 mm Receiver RxA3 front-

end and the ACSIS backend throughout semesters 10A and 10B. Each core was observed in position-switching mode with an off-position located (-300,-300) arcseconds (in the J2000 coordinate frame) from the core position (see Table 1). ACSIS was configured to cover two 250 MHz-wide windows, one centered on  $\text{HCO}^+$  (3-2) at 267.558 GHz and another centered on  $\text{H}^{13}\text{CO}^+$  (3-2) at 260.255 GHz. Each window was divided into 8192 channels for a resolution of  $\sim 0.05 \text{ km s}^{-1}$ . Each core was observed for about 45 minutes of integration and the beam size of the observations was  $\sim 20''$  FWHM. The JCMT beam size is fairly well matched to the beam sizes of the  $\text{N}_2\text{H}^+$  (1-0) and  $\text{N}_2\text{D}^+$  (2-1) observations presented in Crapsi et al. (2005), i.e.,  $26''$  and  $16''$  FWHM, respectively.

After acquisition, the data were reduced using the Starlink package. Each integration was first visually checked for baseline ripples and extremely large spikes, and such data were removed from the ensemble, if necessary. Spectral baselines were subtracted, frequency axes converted to velocities, and spectra edges trimmed using Starlink scripts kindly provided by T. van Kempen. The integrations were visually inspected and written out as FITS format files using other standard Starlink routines. The spectra for each core were co-added outside of Starlink, using the IDL programming language. Spectra were converted to main beam brightness temperatures using an assumed efficiency of 0.75<sup>8</sup>.  $\text{HCO}^+$  (3-2) emission was detected towards each core except for L1495A-S, but  $\text{H}^{13}\text{CO}^+$  (3-2) emission was only detected towards a few cores (L1521F, Oph D, L1689B, and L328; see Figures 1a-1d). Hence, the  $\text{H}^{13}\text{CO}^+$  data will not be discussed further in this paper.

## 3. RESULTS

The  $\text{HCO}^+$  spectra were fit with a Gaussian model as well as two simple infall/outflow models, the “two-layer” model from Myers et al. (1996) and the “HILL5” model from De Vries & Myers (2005). The two-layer model describes the case of two regions with differing excitation temperatures (lower for the front, higher for the rear) and identical velocity dispersions and total optical depth. The HILL5 model describes the case of a core whose excitation temperature peaks at the center and falls off linearly with radius. The HILL5 core also has its front and rear halves moving towards or away from each other. Both models reproduce spectra with one peak and a shoulder reasonably well, though the HILL5 model is better than the two-layer model at fitting spectra with two peaks (De Vries & Myers 2005). The five free parameters in both infall/outflow models are inward/outward velocity, kinetic temperature, peak optical depth, velocity dispersion, and velocity with respect to the local standard of rest. The dynamic models assume that the two peaks in the prototypical infall/outflow profile arise from self-absorption and not from having two unrelated sources with slightly different velocities along the same line of sight. This assumption can be tested through observations of an optically thin tracer that should peak at the same velocity as the self-absorption dip in the optically thick spectrum if no radial motion is present. The  $\text{H}^{13}\text{CO}^+$  (3-2) observations described in Section 2 were

<sup>7</sup> The James Clerk Maxwell Telescope is operated by the Joint Astronomy Centre on behalf of the Science and Technology Facilities Council of the UK, the Netherlands Association for Scientific Research, and the National Research Council of Canada

<sup>8</sup> [http://www.jach.hawaii.edu/JCMT/spectral\\_line/Standards/beameff.html](http://www.jach.hawaii.edu/JCMT/spectral_line/Standards/beameff.html)

intended to be this optically thin tracer, but detections were rare. The  $\text{N}_2\text{H}^+$  and  $\text{N}_2\text{D}^+$  observations presented in Crapsi et al. (2005) are sufficient to show that there are no confounding superpositions in our sample. In the relatively few cases where  $\text{H}^{13}\text{CO}^+$  (3-2) is detected, the line peaks at the same velocity as the  $\text{N}_2\text{H}^+$  and  $\text{N}_2\text{D}^+$  spectra. The Gaussian and dynamic models were fit with the MPFIT suite of functions (Markwardt 2009).

For each core, the Gaussian and dynamic model fits were compared with F-tests, taking into account the chi-squared values for the fits and the degrees of freedom in the fits. For those cores where the F-test prefers a dynamic model and the inward/outward motions are at least three times the uncertainty of the motion, we treat the core as having inward or outward motions for the rest of this paper. We describe as ‘static core’ those cores for which the F-test prefers the Gaussian model or the uncertainty in the radial motions is greater than three times the magnitude of the motion. The signal-to-noise ratio of the L1495A-S observations is too low to attempt a fit to either model. The peak intensities, integrated intensities, and velocity dispersions (standard deviations, or  $\sigma$  for a Gaussian velocity distribution) measured from the best fits to the  $\text{HCO}^+$  spectra are given in Table 1, with the intensities given on  $T_{\text{mb}}$  scale. Note that the cores L1521F and L328 are actually protostellar, not starless, and L1521F has the largest infall velocity in our survey. The infall velocity of L1521F was measured to be  $0.2\text{--}0.3\text{ km s}^{-1}$  by Onishi et al. (1999). The presence of an embedded protostar likely reduces the accuracy of the HILL5 and two-layer models (note the relatively poor fit to the blue peak of the spectrum), so we trust the detailed model of Onishi et al. (1999) to provide a more accurate estimate of the infall velocity than we derive here. The kinematic state and preferred model of each core as determined by the model fits are given in Table 3, along with previous kinematic classifications from the literature (see §4). In Table 3, we also give the velocity with respect to the local standard of rest from the best-fit model to our  $\text{HCO}^+$  spectra, along with the LSR velocity fit to the  $\text{N}_2\text{H}^+$  (1-0) spectra from Crapsi et al. (2005). We find that the median of the absolute value of the velocity difference between the LSR velocity from  $\text{HCO}^+$  and  $\text{N}_2\text{H}^+$  is  $0.07\text{ km s}^{-1}$  with a standard deviation of  $0.1\text{ km s}^{-1}$ . This velocity difference likely comes from velocity gradients along the line of sight due to inward/outward motions, since  $\text{HCO}^+$  and  $\text{N}_2\text{H}^+$  will sometimes probe different layers within a core. The uncertainties given in Table 3 are the  $1\sigma$  standard deviations.

Masses and radii for the cores in this survey were taken from the literature and calculated from (sub)millimeter continuum surveys. Most core masses are derived from the observed flux at  $850\text{ }\mu\text{m}$  or  $1.2\text{ mm}$  using the formula

$$M = 0.12 \left[ e^{\left( \frac{1}{1.439} \frac{\lambda}{\text{mm}} \frac{T}{10\text{ K}} \right)^{-1}} - 1 \right] \left( \frac{\kappa_\nu}{0.01\text{ cm}^2\text{ g}^{-1}} \right)^{-1} \left( \frac{S_\nu}{\text{Jy}} \right) \left( \frac{D}{100\text{ pc}} \right)^2 \left( \frac{\lambda}{\text{mm}} \right)^3 M_\odot. \quad (1)$$

We assume that all cores are isothermal at  $10\text{ K}$ , as assumed in the core mass calculations of Crapsi et al. (2005) and consistent with the average tempera-

tures derived from  $\text{NH}_3$  observations of starless cores (Tafalla et al. 2002; Schnee et al. 2009). Real cores have temperature gradients ranging from  $\sim 13\text{ K}$  at large radii to  $\sim 6\text{ K}$  at the center (e.g., Crapsi et al. 2007; Pagani et al. 2007; Schnee et al. 2007b), but these variations in temperature do not affect the conclusions of this paper. We assume a value of  $\kappa_\nu$  at  $850\text{ }\mu\text{m}$  of  $0.01\text{ cm}^2\text{ g}^{-1}$  and  $\kappa_\nu$  at  $1.2\text{ mm}$  of  $0.005\text{ cm}^2\text{ g}^{-1}$ , as assumed in Sadavoy et al. (2010) and Crapsi et al. (2005), respectively. These values for  $\kappa_\nu$  are consistent with each other for an emissivity spectral index of 2, in agreement with observations of the starless cores L1498 (Shirley et al. 2005) and TMC-1C (Schnee et al. 2010). Distances ( $D$ ) to the cores and references used to determine core masses are given in Table 2. We were unable to find previously published values for the masses and radii of the cores L1495 and L1400A.

Following Sadavoy et al. (2010), we calculate the Jeans mass for the cores in this survey using the formula

$$M_J = 1.9 \left( \frac{T}{10\text{ K}} \right) \left( \frac{R}{0.07\text{ pc}} \right) M_\odot. \quad (2)$$

As in the calculation of core masses, when calculating the Jeans mass we assume that all cores are isothermal at  $T = 10\text{ K}$  and use the radii ( $R$ ) given in Table 2.

#### 4. DISCUSSION

A plot of infall velocity (see Table 3) vs. degree of deuteration (see Table 2) is shown in Figure 2. Nine cores show no evidence for infall or outflow, five cores have outward motions, and eleven have inward motions. Below an  $N(\text{N}_2\text{D}^+)/N(\text{N}_2\text{H}^+)$  ratio of 0.1, there is no correlation with infall velocity. For the eight cores with  $N(\text{N}_2\text{D}^+)/N(\text{N}_2\text{H}^+) \geq 0.1$ , six cores have infall velocities and two cores appear to be static. We therefore find a general trend, though not a quantitative correlation, that inward motions are more likely to be found at higher levels of deuteration whereas at lower levels of deuteration, inward and outward motions are roughly equally likely to be found. The  $\text{HCO}^+$  spectra therefore support the idea that the most chemically evolved starless cores are also dynamically evolved.

Simpson et al. (2011) found that the Jeans stability of a pre-stellar core provides a reasonable predictor of its dynamical state. As shown in Figure 2 (see also Tables 2 and 3), we find that three Jeans-stable cores (those with  $M/M_{\text{Jeans}} < 1$ ) show inward motions, two cores appear to be static, and four show outflow motions. Those cores with  $M/M_{\text{Jeans}} > 1$  are much more likely to have line asymmetries associated with infall (eight cores) than outward motions (no cores), and six cores with  $M/M_{\text{Jeans}} > 1$  are best fit by Gaussian profiles. Our results are in agreement with those of Simpson et al. (2011) in that the Jeans stability of dense cores is a useful indicator of likely infall candidates, and the identification of collapsing cores becomes more likely with increasing  $M/M_{\text{Jeans}}$ . As shown in Figure 2, those cores with  $N(\text{N}_2\text{D}^+)/N(\text{N}_2\text{H}^+) > 0.1$  also have  $M/M_{\text{Jeans}} > 1$ .

Many cores with lower degrees of deuteration, however, also have high  $M/M_{\text{Jeans}}$  (L1495A-S, TMC-1C, CB 23, L1517B, L1689B, L492, and L328) and these cores sometimes exhibit infall motions that are a consequence of their Jeans instability. There are no cores with  $M/M_{\text{Jeans}}$

$< 1$  and  $N(\text{N}_2\text{D}^+)/N(\text{N}_2\text{H}^+) > 0.1$ . Those cores with  $M/M_{\text{Jeans}} > 1$ , but no indication of inward motions, may be supported by mechanisms other than thermal pressure (e.g., turbulent or magnetic pressure). Alternatively, infall may indeed be on-going, but the signature of this motion could be missing from the  $\text{HCO}^+$  (3-2) spectra in some cores due to freeze-out (Roberts et al. 2010) or rotation (Redman et al. 2004). We suggest that those cores with super-Jeans masses but no indication for infall are a good sample for future observations.

The origin of outward motions in five starless cores in our survey, as indicated by negative infall velocities in Table 3 and Figure 2, is not fully understood. Such outward motions have been seen in previous surveys (e.g., Sohn et al. 2007; Lee & Myers 2011) and may indicate oscillatory behavior (Lada et al. 2003; Broderick & Keto 2010). Indeed, oscillatory behavior may also be responsible for some of the inward motions observed in our  $\text{HCO}^+$  survey. SPH simulations of nominally super-Jeans cores modelled as Bonnor-Ebert spheres may oscillate rather than collapse if the exterior temperatures of the cores are high enough (Anathpindika & Di Francesco 2013). As the sometimes-different classifications of cores as ‘expanding’, ‘oscillating’, or ‘contracting’ in Table 3 make clear, observing cores at slightly different positions with different molecular tracers can lead to very different conclusions, an effect which surely adds considerable scatter to plots like Figure 2.

Only three of the sixteen cores included in four surveys of inward and outward motions (Crapsi et al. 2005; Sohn et al. 2007; Lee & Myers 2011, this work) showed the same behaviour in all cases (L1544, L694-2, and L1197, which all show inward motions). Infall in the cores L1544 and L694-2 has been particularly well-studied, with evidence for extended infall at speeds  $\leq 0.1 \text{ km s}^{-1}$  seen in  $\text{N}_2\text{H}^+$  observations (Tafalla et al. 1998; Williams et al. 2006; Keto & Caselli 2010). The lack of a 1:1 correlation between infall velocity and high  $N(\text{N}_2\text{D}^+)/N(\text{N}_2\text{H}^+)$  or  $M/M_{\text{Jeans}}$  is likely to be at least partly a result of the uncertainties in measuring the dynamics of cores with a single molecular tracer at a single position. In addition, because starless cores won’t all reach exactly the same level of  $N(\text{N}_2\text{D}^+)/N(\text{N}_2\text{H}^+)$  just before collapse, one would not expect a perfect correlation with infall even in a comprehensive set of observations.

It may seem surprising that some cores in this survey have significant infall velocities without having similarly large  $N(\text{N}_2\text{D}^+)/N(\text{N}_2\text{H}^+)$  ratios. As mentioned above, in some cases the inward motions may be due to oscillations in a stable core rather than being caused by collapse, in which case the low  $N(\text{N}_2\text{D}^+)/N(\text{N}_2\text{H}^+)$  ratio is a true indicator of the stability of a core. Alternatively,  $\text{HCO}^+$  may be preferentially tracing accretion motions (i.e., motions of material onto the core) instead of contraction or expansion motions of the core itself, as  $\text{HCO}^+$  is also very abundant at low densities (i.e., in the core envelope and the surrounding molecular cloud), unlike  $\text{N}_2\text{H}^+$ . For example, molecular abundances in the contracting core TMC-1C are affected by accretion from its environment, from which it is gaining material rich in  $\text{N}_2\text{H}^+$  but likely not in  $\text{N}_2\text{D}^+$  (Schnee & Goodman 2005; Schnee et al. 2007a). It is also possible that cores with significant infall velocities but low levels of deuterium

fractionation are too young to have significant deuterium enrichment despite their high central densities. For instance, the cores L1521E (Tafalla & Santiago 2004) and L1689B (Lee et al. 2003) have been identified as dense cores with little chemical evolution, likely due to their relative youth ( $\leq 1.5 \times 10^5$  yr). In these chemically young cores, where CO is not highly depleted,  $\text{HCO}^+$  may be a better tracer of infall in the central high density region, compared to chemically evolved cores. Therefore, a mismatch between the chemical and dynamical states of a starless core inferred by this survey could be due to 1) a single  $\text{HCO}^+$  (3-2) spectrum being an incomplete tracer of the dynamics of an oscillating dense core, 2) the  $N(\text{N}_2\text{D}^+)/N(\text{N}_2\text{H}^+)$  ratio within a core being lowered by accretion from the surrounding medium, or 3) the timescale of chemical evolution being significantly longer than the dynamical timescale.

The magnitude of the inward and outward velocities are low, similar to the sound speed ( $\sim 0.2 \text{ km s}^{-1}$  for a 10 K core). This result suggests that the initial conditions from which the motions are derived were near hydrostatic equilibrium. That is, the infall motions are not dominated by highly supersonic flows attributed to cloud turbulence but more likely derive from gravitational collapse of a core that has lost pressure support. The outward motions observed are consistent with either oscillations of a near gravitational equilibrium object (Broderick & Keto 2010; Anathpindika & Di Francesco 2013) or thermal expansion of an over-pressured but gravitationally unbound core, as would be expected for a core with  $M/M_{\text{Jeans}} \lesssim 1$ .

## 5. FUTURE WORK

As outlined in this paper, there is a need for a uniform multidimensional study of the kinematics and chemistry of dense cores. The work presented in this paper is limited by the single-pointing observations. Spectral line maps would be better able to determine the location of peak infall or outflow, and to determine whether a core shows infall or outflow spectral signatures consistently across its extent. Part of the difference between the infall surveys presented in Table 3 can be attributed to the different pointing centers of the observations. To the extent that the velocity field changes across a core, these positional differences will confuse the conclusions of pointed surveys. Furthermore, the ‘center’ of a core is not always a well-defined location. For example the center of L183 is offset by  $\sim 20''$  between the studies of Crapsi et al. (2005) and Pagani et al. (2007). A second conclusion that can be drawn from Table 3 is that there is no single best molecular tracer of inward and outward motions in dense cores. Although  $\text{HCO}^+$  is relatively bright and shows infall motion clearly in many cores, it may not trace the regions in starless cores with the lowest temperatures, highest densities, and most depletion. In this case, the infall velocity measured from  $\text{HCO}^+$  spectra is likely to be an underestimate of the maximum infall speed. To map precisely the inward and/or outward motions in a core, one would want to have several spectral maps with different molecules and rotational transitions. These observations could then be modeled with a radiative transfer code to constrain self-consistently the density, temperature, chemistry, and kinematic profiles of the cores. Such a survey would require a substantial

amount of observing time. We note that the pointed observations of a single infall tracer in this paper required over 30 hours of telescope time (including overheads) over multiple semesters with the JCMT. The combination of high sensitivity with high spatial and spectral resolution provided by the Atacama Large Millimeter/submillimeter Array (ALMA) may make it possible to carry out a comprehensive survey of the connection between the chemistry, kinematics, and role of environment in dense cores.

## 6. SUMMARY

Crapsi et al. (2005) predicted that dense cores with  $N(\text{N}_2\text{D}^+)/N(\text{N}_2\text{H}^+) > 0.1$  will show evidence for infall. To test this hypothesis, we observed  $\text{HCO}^+$  (3-2) towards the Crapsi et al. (2005) sample of 26 dense cores (24 starless and 2 protostellar) and analyzed the spectra to look for inward and outward motions. We find that those cores with the largest values of  $N(\text{N}_2\text{D}^+)/N(\text{N}_2\text{H}^+)$  and  $M/M_{\text{Jeans}}$  are indeed more likely to show the signature of infall than the population as a whole, though some cores that have lower levels of deuterium fractionation and greater Jeans stability also show inward motions. Since asymmetries from inward and outward motions vary by position within cores (Lee et al. 2001; Lada et al. 2003) and vary by tracer observed (e.g., Lee & Myers 2011), it is not surprising that we do not see very tight correlations between the degree of deuterium fractionation or Jeans stability with infall velocity. The presence of outward motions, and perhaps some of the inward motions, in these presumably long-lived cores is possibly a result of oscillations (Lada et al. 2003; Broderick & Keto 2010; Anathpindika & Di Francesco 2013) and such outward motions have been seen before in previous surveys of dense cores (e.g., Sohn et al. 2007; Lee & Myers 2011). The magnitudes of the inward and outward motions are on the order of the sound speed, suggesting that the cores formed near hydrostatic equilibrium rather than out of supersonic flows.

We thank Malcolm Currie for his help reducing JCMT spectra. We thank our anonymous referee for suggestions that have significantly improved the clarity and content of this paper. The National Radio Astronomy Observatory is a facility of the National Science Foundation operated under cooperative agreement by Associated Universities, Inc. JDF and DJ acknowledge support by the National Research Council of Canada and the Natural Sciences and Engineering Council of Canada (NSERC) via a Discovery Grant. AP is partially supported by the NSERC graduate scholarship program. RF is a Dunlap Fellow at the Dunlap Institute for Astronomy and Astrophysics, University of Toronto. The Dunlap Institute is funded through an endowment established by the David Dunlap family and the University of Toronto. The James Clerk Maxwell Telescope is operated by the Joint Astronomy Centre on behalf of the Science and Technology Facilities Council of the United Kingdom, the Netherlands Organisation for Scientific Research, and the National Research Council of Canada. The JCMT program ID numbers associated with this project are M10AC002, M10BC001, and M11BC003. This research has made use of the SIMBAD database, operated at CDS, Strasbourg, France.

*Facilities:* JCMT

## REFERENCES

- Anathpindika, S., & Di Francesco, J. 2013, arXiv:1301.0240  
 Bourke, T. L., Myers, P. C., Evans, N. J., II, et al. 2006, *ApJ*, 649, L37  
 Broderick, A. E., & Keto, E. 2010, *ApJ*, 721, 493  
 Caselli, P., Vastel, C., Ceccarelli, C., et al. 2008, *A&A*, 492, 703  
 Crapsi, A., De Vries, C. H., Huard, T. L., et al. 2005, *A&A*, 439, 1023  
 Crapsi, A., Caselli, P., Walmsley, M. C., & Tafalla, M. 2007, *A&A*, 470, 221  
 De Vries, C. H., & Myers, P. C. 2005, *ApJ*, 620, 800  
 Di Francesco, J., Evans, N. J., II, Caselli, P., et al. 2007, *Protostars and Planets V*, 17  
 Di Francesco, J., Johnstone, D., Kirk, H., MacKenzie, T., & Ledwosinska, E. 2008, *ApJS*, 175, 277  
 Emprechtinger, M., Caselli, P., Volgenau, N. H., Stutzki, J., & Wiedner, M. C. 2009, *A&A*, 493, 89  
 Enoch, M. L., Evans, N. J., II, Sargent, A. I., et al. 2008, *ApJ*, 684, 1240  
 Evans, N. J., II 1999, *ARA&A*, 37, 311  
 Friesen, R. K., Kirk, H. M., & Shirley, Y. L. 2013, *ApJ*, 765, 59  
 Gregersen, E. M., & Evans, N. J., II 2000, *ApJ*, 538, 260  
 Hatchell, J., Fuller, G. A., Richer, J. S., Harries, T. J., & Ladd, E. F. 2007, *A&A*, 468, 1009  
 Hirota, T., Maezawa, H., & Yamamoto, S. 2004, *ApJ*, 617, 399  
 Kauffmann, J., Bertoldi, F., Bourke, T. L., Evans, N. J., II, & Lee, C. W. 2008, *A&A*, 487, 993  
 Keto, E., & Caselli, P. 2010, *MNRAS*, 402, 1625  
 Lada, C. J., Bergin, E. A., Alves, J. F., & Huard, T. L. 2003, *ApJ*, 586, 286  
 Lee, C. W., & Myers, P. C. 1999, *ApJS*, 123, 233  
 Lee, C. W., Myers, P. C., & Tafalla, M. 1999, *ApJ*, 526, 788  
 Lee, C. W., Myers, P. C., & Tafalla, M. 2001, *ApJS*, 136, 703  
 Lee, J.-E., Evans, N. J., II, Shirley, Y. L., & Tatematsu, K. 2003, *ApJ*, 583, 789  
 Lee, C. W., Bourke, T. L., Myers, P. C., et al. 2009, *ApJ*, 693, 1290  
 Lee, C. W., & Myers, P. C. 2011, *ApJ*, 734, 60  
 Markwardt, C. B. 2009, *Astronomical Data Analysis Software and Systems XVIII*, 411, 251  
 Myers, P. C., Mardones, D., Tafalla, M., Williams, J. P., & Wilner, D. J. 1996, *ApJ*, 465, L133  
 Nutter, D., & Ward-Thompson, D. 2007, *MNRAS*, 374, 1413  
 Oliveira, C. M., Hébrard, G., Howk, J. C., et al. 2003, *ApJ*, 587, 235  
 Onishi, T., Mizuno, A., & Fukui, Y. 1999, *PASJ*, 51, 257  
 Pagani, L., Bacmann, A., Cabrit, S., & Vastel, C. 2007, *A&A*, 467, 179  
 Redman, M. P., Keto, E., Rawlings, J. M. C., & Williams, D. A. 2004, *MNRAS*, 352, 1365  
 Roberts, J. F., Rawlings, J. M. C., & Stace, H. A. 2010, *MNRAS*, 408, 2426  
 Sadavoy, S. I., Di Francesco, J., & Johnstone, D. 2010, *ApJ*, 718, L32  
 Schnee, S., & Goodman, A. 2005, *ApJ*, 624, 254  
 Schnee, S., Caselli, P., Goodman, A., et al. 2007, *ApJ*, 671, 1839  
 Schnee, S., Kauffmann, J., Goodman, A., & Bertoldi, F. 2007, *ApJ*, 657, 838  
 Schnee, S., Rosolowsky, E., Foster, J., Enoch, M., & Sargent, A. 2009, *ApJ*, 691, 1754  
 Schnee, S., Enoch, M., Noriega-Crespo, A., et al. 2010, *ApJ*, 708, 127  
 Schnee, S., Di Francesco, J., Enoch, M., et al. 2012, *ApJ*, 745, 18  
 Shirley, Y. L., Nordhaus, M. K., Grcevich, J. M., et al. 2005, *ApJ*, 632, 982  
 Simpson, R. J., Johnstone, D., Nutter, D., Ward-Thompson, D., & Whitworth, A. P. 2011, *MNRAS*, 417, 216  
 Sohn, J., Lee, C. W., Park, Y.-S., et al. 2007, *ApJ*, 664, 928  
 Stutz, A. M., Rieke, G. H., Bieging, J. H., et al. 2009, *ApJ*, 707, 137  
 Tafalla, M., Mardones, D., Myers, P. C., et al. 1998, *ApJ*, 504, 900  
 Tafalla, M., Myers, P. C., Caselli, P., Walmsley, C. M., & Comito, C. 2002, *ApJ*, 569, 815

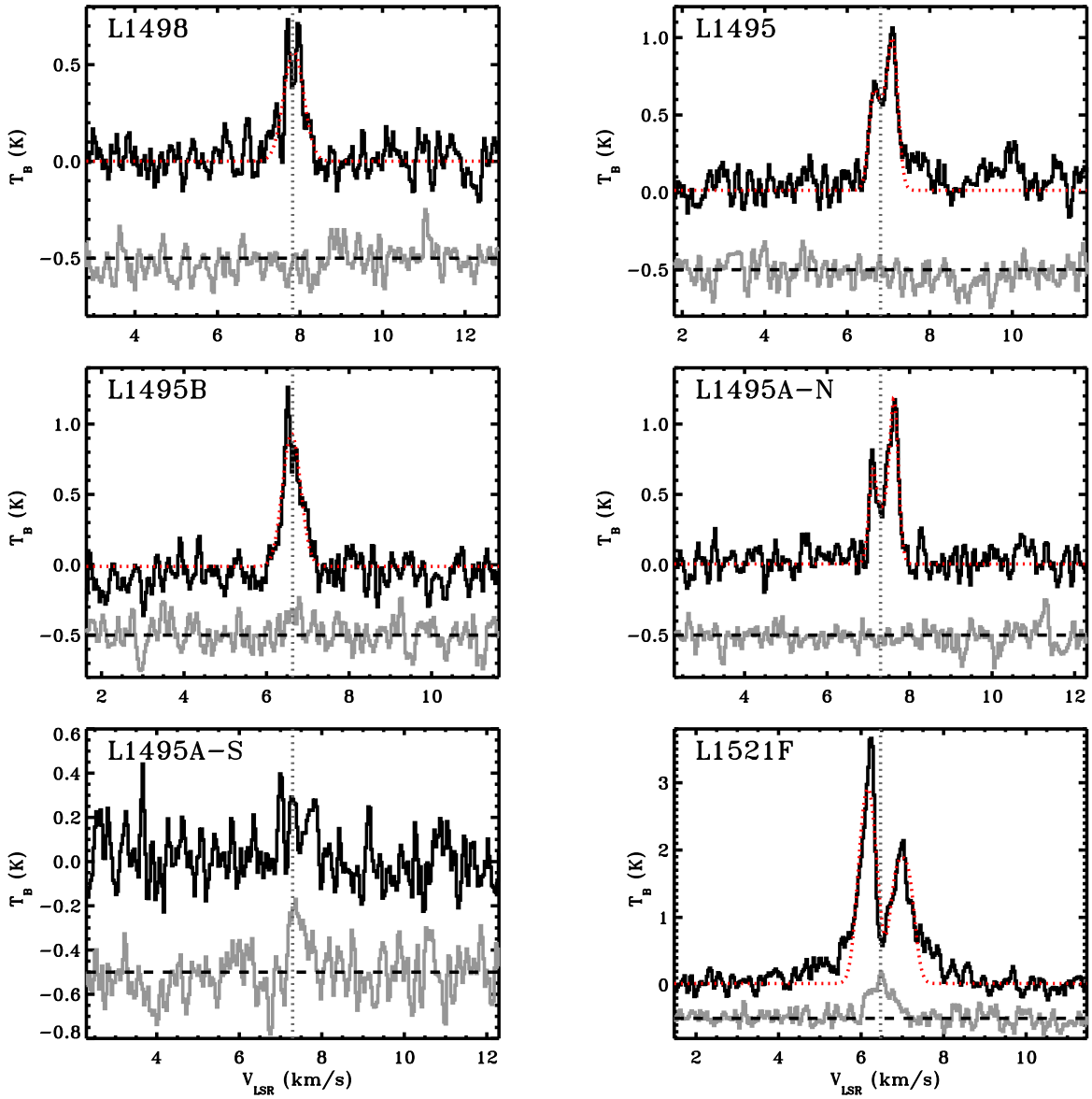


**Figure 1a.** Observed  $\text{HCO}^+$  (3-2) spectra (black) and  $\text{H}^{13}\text{CO}^+$  (3-2) spectra (grey) for the cores L1498, L1495, L1495B, L1495A-N, L1495A-S, and L1521F. The dotted vertical line shows the LSR velocities of  $\text{N}_2\text{H}^+$  (1-0) (Crapsi et al. 2005). The  $\text{H}^{13}\text{CO}^+$  spectra are offset by  $-0.5$  K, with a dashed horizontal line showing the zero level of the  $\text{H}^{13}\text{CO}^+$  spectra. The red dotted lines shows the best fit to the observed  $\text{HCO}^+$  (3-2) spectra.

Tafalla, M., & Santiago, J. 2004, *A&A*, 414, L53  
 Williams, J. P., & Myers, P. C. 1999, *ApJ*, 511, 208

Williams, J. P., Lee, C. W., & Myers, P. C. 2006, *ApJ*, 636, 952

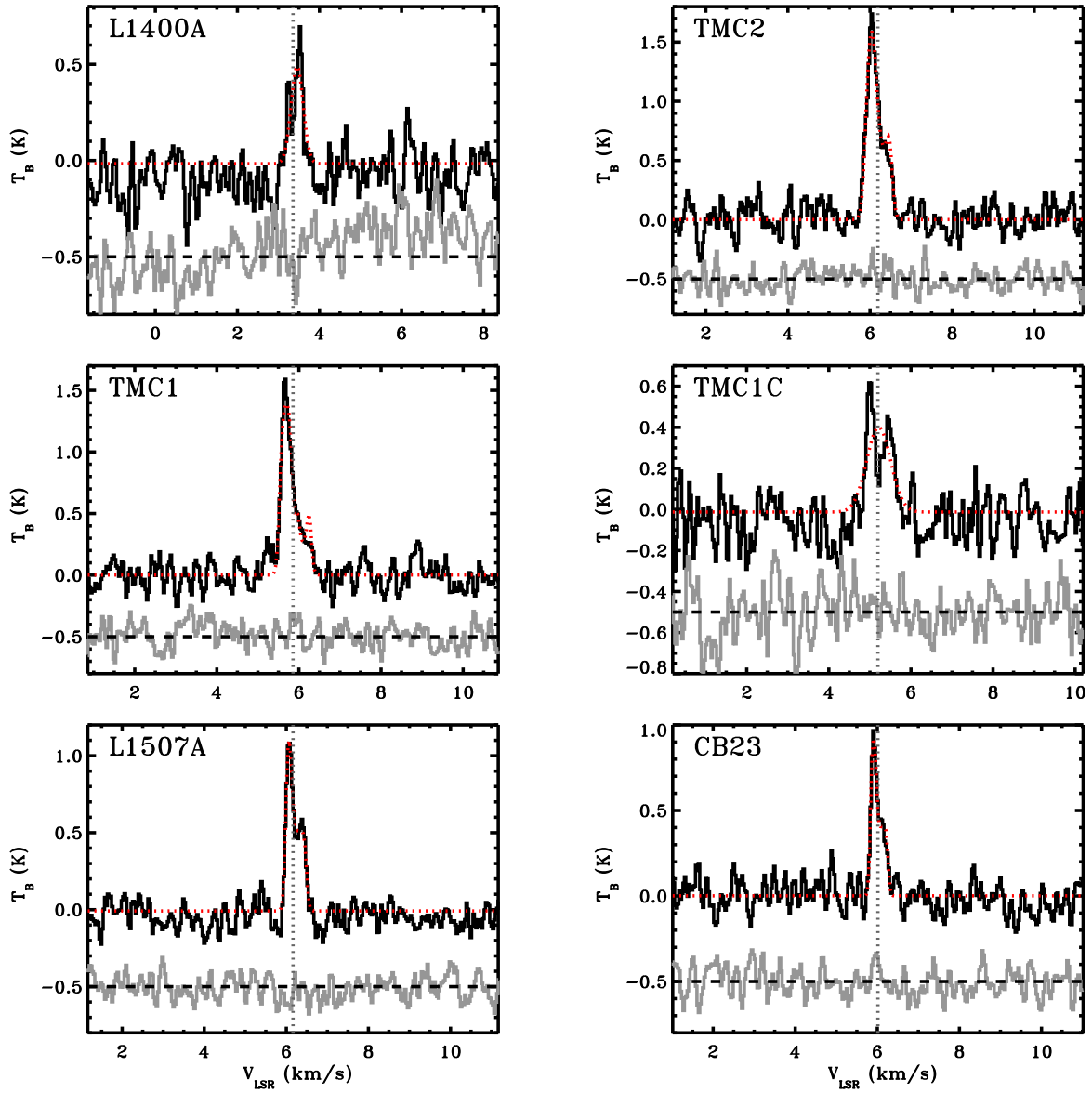


**Figure 1b.** Same as Figure 1a, for the cores L1400A, TMC2, TMC1, TMC1C, L1507A, and CB23.

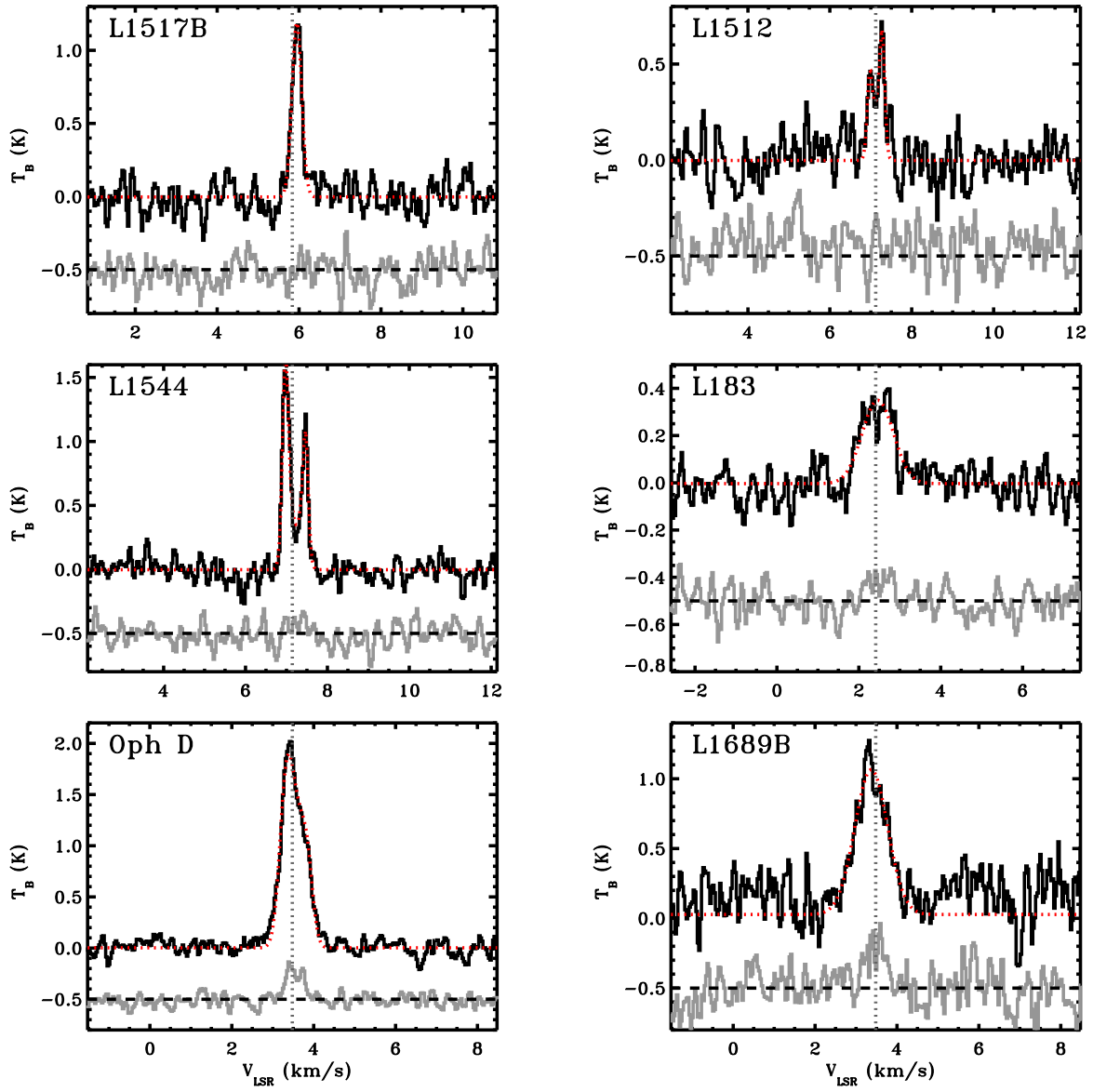


Figure 1c. Same as Figure 1a, for the cores L1517B, L1512, L1544, L183, Oph D, and L1689B.



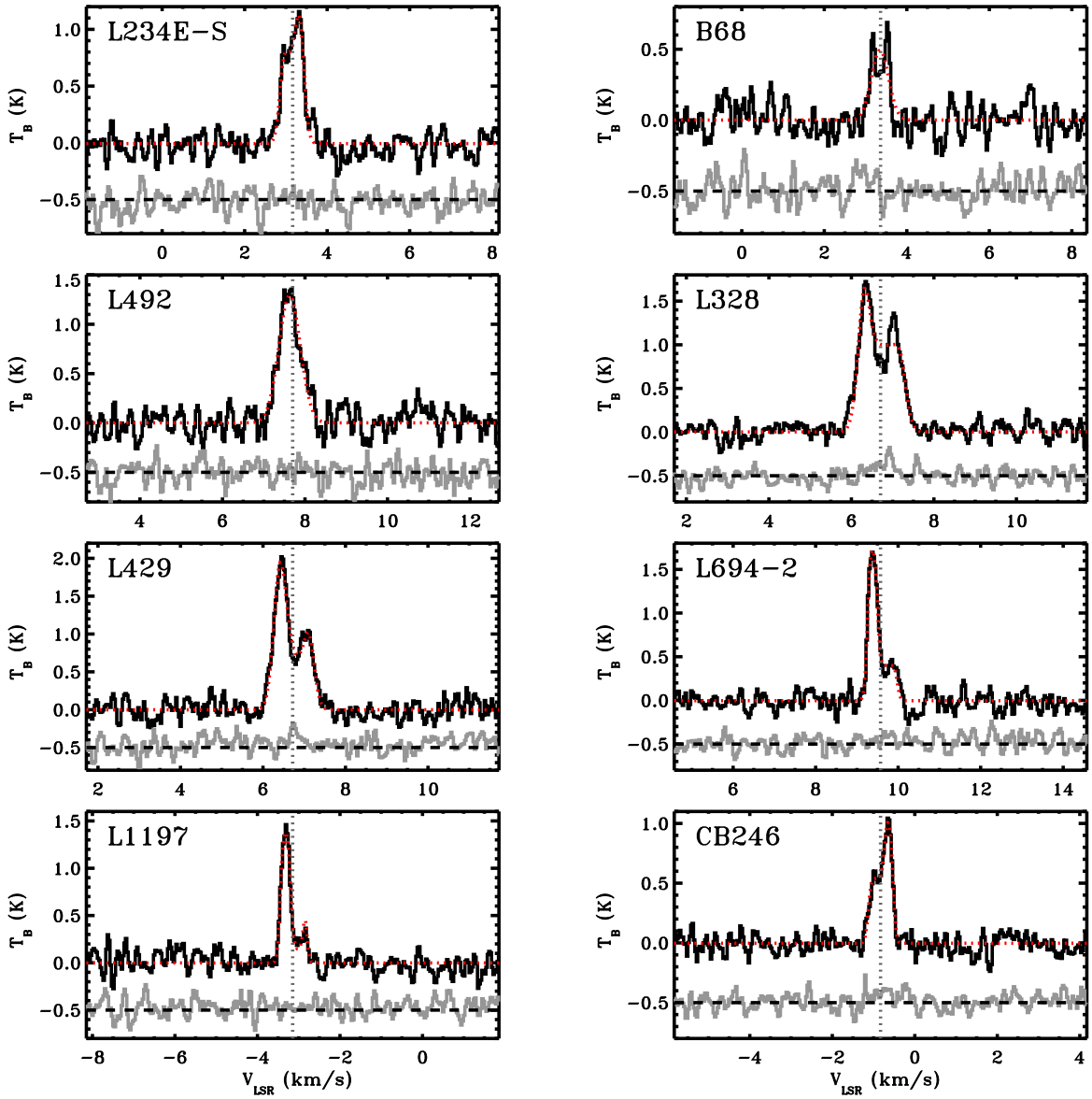
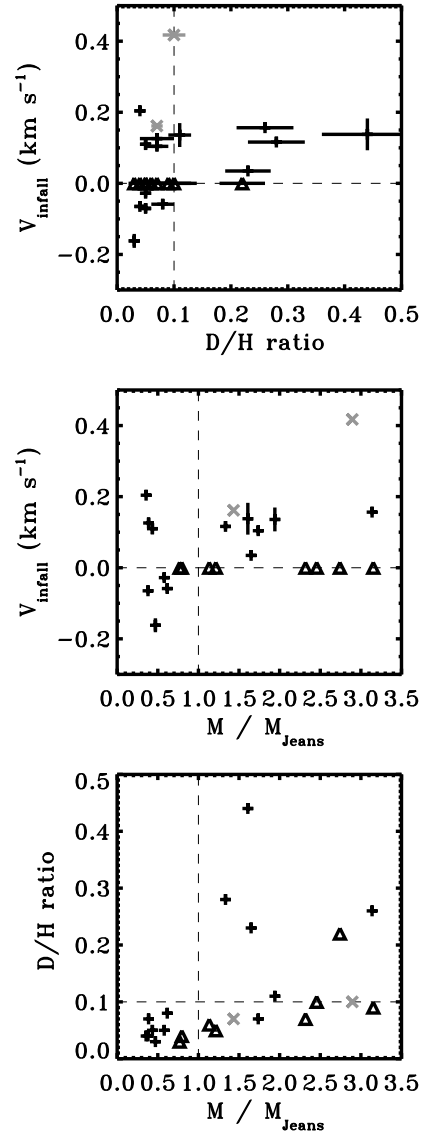


Figure 1d. Same as Figure 1a, for the cores L234E-S, B68, L492, L328, L429, L694-2, L1197, and CB 246.



**Figure 2.** Infall velocity plotted against the  $N(\text{N}_2\text{D}^+)/N(\text{N}_2\text{H}^+)$  from Crapsi et al. (2005) (*top*) and the ratio of the core mass to the thermal Jeans mass, as calculated from Equations 1 and 2 and reported in Table 2 (*middle*). Positive values of  $V_{\text{infall}}$  indicate inward motions. The  $N(\text{N}_2\text{D}^+)/N(\text{N}_2\text{H}^+)$  ratio against the  $M/M_{\text{J}}$  ratio is plotted in the bottom panel. The protostellar cores L328 and L1521F are represented by grey 'x' symbols and all of the other cores are thought to be starless. “Static cores” are given an infall/outflow velocity of  $0 \text{ km s}^{-1}$  and are represented by triangles. The cores L1495 and L1400A are not plotted in the middle and bottom panels because we could not determine  $M/M_{\text{J}}$  for them from the literature. The core L1495A-S is not plotted in any panel because we did not detect it in our  $\text{HCO}^+$  observations.

**Table 1**  
Summary of HCO<sup>+</sup> Observations

Name	RA <sup>1</sup> J2000	Dec <sup>1</sup> J2000	Peak Intensity T <sub>mb</sub> (K)	Integrated Intensity T <sub>mb</sub> (K km s <sup>-1</sup> )	Velocity Dispersion km s <sup>-1</sup>	rms T <sub>mb</sub> (K)
L1498	04:10:51.5	+25:09:58	0.57	0.34	0.24	0.08
L1495	04:14:11.2	+28:08:56	1.00	0.58	0.16	0.09
L1495B <sup>2</sup>	04:18:05.1	+28:22:22	0.93	0.52	0.22	0.11
L1495A-N	04:18:31.8	+28:27:30	1.17	0.57	0.14	0.09
L1495A-S	04:18:41.8	+28:23:50	N/A	N/A	N/A	0.10
L1521F <sup>3</sup>	04:28:39.1	+26:51:35	2.91	2.73	0.19	0.10
L1400A	04:30:56.8	+54:52:36	0.49	0.19	0.15	0.14
TMC 2	04:32:48.7	+24:25:52	1.59	0.71	0.11	0.11
TMC 1	04:41:32.9	+25:44:44	1.39	0.61	0.09	0.11
TMC 1C	04:41:38.8	+26:00:22	0.40	0.30	0.29	0.11
L1507A	04:42:38.6	+29:43:45	1.10	0.37	0.08	0.08
CB 23	04:43:27.7	+29:39:11	0.92	0.26	0.07	0.07
L1517B	04:55:17.6	+30:37:49	1.19	0.35	0.12	0.09
L1512	05:04:09.7	+32:43:09	0.68	0.22	0.09	0.10
L1544	05:04:16.6	+25:10:48	1.66	0.61	0.12	0.08
L183	15:54:08.4	-02:52:23	0.35	0.34	0.38	0.06
Oph D	16:28:28.9	-24:19:19	1.90	1.29	0.17	0.06
L1689B	16:34:45.8	-24:37:50	1.06	1.04	0.40	0.16
L234E-S	16:48:08.6	-10:57:25	1.13	0.59	0.14	0.09
B68	17:22:38.9	-23:49:46	0.49	0.26	0.21	0.09
L492	18:15:47.4	-03:45:53	1.29	0.84	0.26	0.13
L328 <sup>4</sup>	18:17:00.4	-18:01:52	1.65	1.43	0.22	0.09
L429	18:17:05.1	-08:13:40	1.94	1.30	0.19	0.10
L694-2	19:41:04.5	+10:57:02	1.72	0.63	0.10	0.10
L1197	22:37:02.3	+58:57:21	1.38	0.46	0.09	0.10
CB 246	23:56:41.5	+58:34:09	1.00	0.44	0.10	0.07

<sup>1</sup> From Crapsi et al. (2005)

<sup>2</sup> Name and coordinates from Lee & Myers (1999), not to be confused with LDN 1495B with J2000 coordinates 04:15:36.5 +28:46:06

<sup>3</sup> Protostellar (Bourke et al. 2006)

<sup>4</sup> Protostellar (Lee et al. 2009)

**Table 2**  
Summary of Properties from Literature

Name	Distance pc	$N(N_2D^+)/N(N_2H^+)^1$	Radius "	Radius pc	Mass $M_\odot$	$M_J$ $M_\odot$	$M/M_J$
L1498	140 <sup>1</sup>	$0.04 \pm 0.01$	56.0 <sup>3</sup>	0.038	0.8 <sup>3</sup>	1.0	0.8
L1495	140 <sup>1</sup>	$0.05 \pm 0.01$	... <sup>4</sup>	...	... <sup>4</sup>	...	...
L1495B	140 <sup>1</sup>	$0.10 \pm 0.04$	92.8 <sup>5</sup>	0.063	4.2 <sup>5</sup>	1.7	2.5
L1495A-N	140 <sup>1</sup>	$0.04 \pm 0.01$	15.5 <sup>3</sup>	0.010	0.1 <sup>3</sup>	0.3	0.3
L1495A-S	140 <sup>1</sup>	$0.08 \pm 0.03$	20.9 <sup>3</sup>	0.014	0.7 <sup>3</sup>	0.4	1.7
L1521F <sup>7</sup>	140 <sup>1</sup>	$0.10 \pm 0.02$	83.0 <sup>3</sup>	0.056	4.4 <sup>3</sup>	1.5	2.9
L1400A	140 <sup>1</sup>	$0.05 \pm 0.02$	... <sup>4</sup>	...	... <sup>4</sup>	...	...
TMC 2	140 <sup>1</sup>	$0.11 \pm 0.02$	230.6 <sup>2</sup>	0.156	8.2 <sup>2</sup>	4.2	2.0
TMC 1	140 <sup>1</sup>	$0.04 \pm 0.01$	31.9 <sup>3</sup>	0.022	0.2 <sup>3</sup>	0.6	0.3
TMC 1C	140 <sup>1</sup>	$0.07 \pm 0.02$	87.1 <sup>3</sup>	0.059	3.7 <sup>3</sup>	1.6	2.3
L1507A	140 <sup>1</sup>	$0.05 \pm 0.01$	45.2 <sup>3</sup>	0.031	0.4 <sup>3</sup>	0.8	0.5
CB 23	140 <sup>1</sup>	$0.07 \pm 0.02$	78.0 <sup>6</sup>	0.053	2.5 <sup>6</sup>	1.4	1.8
L1517B	140 <sup>1</sup>	$0.06 \pm 0.01$	77.1 <sup>3</sup>	0.052	1.6 <sup>3</sup>	1.4	1.1
L1512	140 <sup>1</sup>	$0.05 \pm 0.01$	47.5 <sup>3</sup>	0.032	0.5 <sup>3</sup>	0.9	0.6
L1544	140 <sup>1</sup>	$0.23 \pm 0.04$	60.1 <sup>3</sup>	0.041	1.8 <sup>3</sup>	1.1	1.6
L183	165 <sup>1</sup>	$0.22 \pm 0.04$	71.3 <sup>3</sup>	0.057	4.3 <sup>3</sup>	1.6	2.7
Oph D	165 <sup>1</sup>	$0.44 \pm 0.08$	55.3 <sup>3</sup>	0.055	1.9 <sup>3</sup>	1.2	1.6
L1689B	165 <sup>1</sup>	$0.09 \pm 0.04$	78.4 <sup>3</sup>	0.063	5.4 <sup>3</sup>	1.7	3.2
L234E-S	165 <sup>1</sup>	$0.08 \pm 0.02$	27.7 <sup>3</sup>	0.022	0.4 <sup>3</sup>	0.6	0.7
B68	125 <sup>1</sup>	$0.03 \pm 0.01$	57.5 <sup>3</sup>	0.035	0.7 <sup>3</sup>	1.0	0.7
L492	200 <sup>1</sup>	$0.05 \pm 0.01$	161.1 <sup>2</sup>	0.156	5.2 <sup>2</sup>	4.2	1.2
L328 <sup>8</sup>	200 <sup>1</sup>	$0.07 \pm 0.01$	31.7 <sup>3</sup>	0.031	1.2 <sup>3</sup>	0.8	1.5
L429	200 <sup>1</sup>	$0.28 \pm 0.05$	19.4 <sup>3</sup>	0.019	0.7 <sup>3</sup>	0.5	1.4
L694-2	250 <sup>1</sup>	$0.26 \pm 0.05$	66.4 <sup>3</sup>	0.080	6.8 <sup>3</sup>	2.2	3.1
L1197	140 <sup>3</sup>	$0.07 \pm 0.03$	19.1 <sup>3</sup>	0.013	0.3 <sup>3</sup>	0.8	0.4
CB 246	140 <sup>1</sup>	$0.03 \pm 0.01$	27.9 <sup>3</sup>	0.019	0.2 <sup>3</sup>	0.5	0.4

<sup>1</sup> (Crapsi et al. 2005)<sup>2</sup> (Kauffmann et al. 2008)<sup>3</sup> (Di Francesco et al. 2008)<sup>4</sup> Core mass and radius not found in the literature<sup>5</sup> (Hirota et al. 2004)<sup>6</sup> (Stutz et al. 2009)<sup>7</sup> Protostellar (Bourke et al. 2006)<sup>8</sup> Protostellar (Lee et al. 2009)

**Table 3**  
Summary of Velocity Information

Name	HCO <sup>+</sup> (3-2) $V_{\text{in/out}}^5$ (km s <sup>-1</sup> ) This work	Model Type	HCN (1-0) Classification (Sohn et al. 2007)	CS, HCN, and N <sub>2</sub> H <sup>+</sup> Classification (Lee & Myers 2011)	N <sub>2</sub> H <sup>+</sup> (1-0) Skewness <sup>5</sup> (km s <sup>-1</sup> ) (Crapsi et al. 2005)	HCO <sup>+</sup> (3-2) $V_{\text{LSR}}$ (km s <sup>-1</sup> ) This work	N <sub>2</sub> H <sup>+</sup> (1-0) $V_{\text{LSR}}$ (km s <sup>-1</sup> ) (Crapsi et al. 2005)
L1498	static core	Gaussian	“contracting core” <sup>2</sup>	“contracting core”	-0.01 ± 0.05	7.85 ± 0.01	7.822 ± 0.001
L1495	-0.07 ± 0.01	Hill 5	...	...	0.10 ± 0.05	6.89 ± 0.01	6.807 ± 0.001
L1495B	static core	Gaussian	...	“static core”	...	6.68 ± 0.01	6.633 ± 0.008
L1495A-N	-0.07 ± 0.01	Hill 5	“contracting core” <sup>1</sup>	“oscillating core”	-0.04 ± 0.05	7.40 ± 0.01	7.296 ± 0.003
L1495A-S	non-detection	...	“contracting core” <sup>2</sup>	“contracting core”	...	non-detection	7.294 ± 0.007
L1521F <sup>6</sup>	0.42 ± 0.01	Hill 5	“contracting core” <sup>1</sup>	“expanding core”	0.19 ± 0.06	6.58 ± 0.01	6.472 ± 0.001
L1400A	static core	Gaussian	“expanding core” <sup>3</sup>	“static core”	...	3.40 ± 0.01	3.355 ± 0.002
TMC 2	0.14 ± 0.03	Hill 5	“contracting core” <sup>2</sup>	“contracting core”	-0.01 ± 0.05	6.20 ± 0.01	6.193 ± 0.001
TMC 1	0.20 ± 0.01	Hill 5	“contracting core” <sup>2</sup>	“contracting core”	-0.13 ± 0.06	5.90 ± 0.01	5.856 ± 0.003
TMC 1C	static core	Gaussian	...	...	0.43 ± 0.10	5.24 ± 0.01	5.196 ± 0.003
L1507A	0.11 ± 0.02	Two Layer	“contracting core” <sup>2</sup>	“oscillating core”	...	6.35 ± 0.01	6.163 ± 0.004
CB 23	0.10 ± 0.01	Two Layer	“contracting core” <sup>2</sup>	“static core”	...	6.15 ± 0.01	6.015 ± 0.002
L1517B	static core	Gaussian	“expanding core” <sup>3</sup>	“static core”	-0.08 ± 0.05	5.95 ± 0.01	5.835 ± 0.001
L1512	-0.03 ± 0.01	Hill 5	“expanding core” <sup>3</sup>	“oscillating core”	0.02 ± 0.05	7.13 ± 0.01	7.121 ± 0.001
L1544	0.03 ± 0.01	Hill 5	“contracting core” <sup>1</sup>	“contracting core”	0.40 ± 0.09	7.21 ± 0.01	7.143 ± 0.002
L183	static core	Gaussian	“oscillating core” <sup>4</sup>	“contracting core”	0.09 ± 0.05	2.22 ± 0.09	2.413 ± 0.001
Oph D	0.14 ± 0.04	Hill 5	“contracting core” <sup>2</sup>	“static core”	0.54 ± 0.12	3.54 ± 0.01	3.478 ± 0.001
L1689B	static core	Gaussian	“contracting core” <sup>1</sup>	“contracting core”	...	3.37 ± 0.01	3.481 ± 0.005
L234E-S	-0.06 ± 0.01	Hill 5	“oscillating core” <sup>4</sup>	“contracting core”	-0.25 ± 0.07	3.16 ± 0.01	3.164 ± 0.003
B68	static core	Gaussian	...	...	-0.09 ± 0.05	3.35 ± 0.02	3.364 ± 0.001
L492	static core	Gaussian	“contracting core” <sup>1</sup>	“contracting core”	0.25 ± 0.07	7.63 ± 0.01	7.701 ± 0.001
L328 <sup>7</sup>	0.16 ± 0.01	Two Layer	...	...	-0.02 ± 0.08	6.91 ± 0.01	6.707 ± 0.002
L429	0.12 ± 0.01	Hill 5	“oscillating core” <sup>4</sup>	“expanding core”	-0.20 ± 0.10	6.72 ± 0.01	6.719 ± 0.001
L694-2	0.16 ± 0.01	Two Layer	“contracting core” <sup>1</sup>	“contracting core”	0.22 ± 0.07	9.77 ± 0.01	9.574 ± 0.001
L1197	0.13 ± 0.01	Hill 5	“contracting core” <sup>2</sup>	“contracting core”	0.08 ± 0.11	-3.14 ± 0.01	-3.147 ± 0.002
CB 246	-0.16 ± 0.02	Two Layer	“oscillating core” <sup>4</sup>	“expanding core”	0.02 ± 0.05	-0.99 ± 0.02	-0.830 ± 0.001

<sup>1</sup> All three hyperfine components of HCN (1-0) show infall

<sup>2</sup> Some hyperfine components of HCN (1-0) show infall

<sup>3</sup> Some hyperfine components of HCN (1-0) show outflow

<sup>4</sup> At least one of the three hyperfine components of HCN (1-0) shows inward motions and at least one of the three hyperfine components shows outward motions

<sup>5</sup> Positive values indicate inward motion, negative values indicate outward motion

<sup>6</sup> Protostellar (Bourke et al. 2006)

<sup>7</sup> Protostellar (Lee et al. 2009)